Determination Of Visibility Time For Geodesic Satellites Orbiting The Earth On Circular Orbit Subject To Minimum Zenith Angle Restriction

Ubong Ukomi[1]
Department of Electrical and Electronic Engineering,
Akwa Ibom State University, Mkpat Enin, Akwa Ibom State

Young, Emem Godwin[2]
Department of Computer Engineering
Akwa Ibom State Polytechnic , Ikot Osurua Ikot Ekpene

Uchegbu, C. E[3]
Dept. of Electrical and Electronic Engineering,
Abia State University, Uturu

***Abstract*— In this paper, determination of visibility time for geodesic satellites orbiting the earth on circular orbit subject to minimum zenith angle restriction is presented. The visibility time analytical expression is derived with respect to orbital altitude or orbital height of the satellite along with minimum zenith angle restriction. The numerical examples are presented with respect to three geodetic satellites, namely; LAGEOS-1, JASON 3 and TANDEM X. The orbital altitude of TanDEM-X satellite is 508.41 km which is the lowest among the three satellites. Notably, the orbital altitude of the Lageos-1 satellite is about 11.6 times that of the TanDEM-X satellite while that of Jason-3 satellite is about 2.6 times the altitude of the TanDEM-X satellite. The results show that among the three geodesic satellites considered, TanDEM-X satellite with the lowest altitude has the lowest visibility time. Also, with minimum zenith angle restriction value of 0°, the Lageos-1 satellite has the maximum visibility time of 73.5 minutes along with the highest visibility angle of 58.7°. The visibility time and visibility angle of the Lageos-1 satellite drop to 51.1 minutes and 40.8° at minimum zenith angle restriction value of 20°. The analytical models that relates the visibility time of each of the satellites with the minimum zenith angle restriction are also derived. In all, the results show that the higher the orbital altitude, the higher the visibility time of the satellite. Also, the minimum zenith angle restriction significantly affect the visibility time of the satellite; notably, the visibility time decreases as the value of minimum zenith angle restriction increases.**

Keywords — Visibility Time, Circular Orbit, Minimum Zenith Angle Restriction, Geodesic, Satellites, Orbit

1. Introduction

Geodesy is a science with major focus on measurement and establishment of clear understanding of the basic earth properties, namely; the earth geometry, the earth gravitational rotation, the gravity and the geoid [1,2, 3,4, 5,6, 7,8, 9,10, 11]. Such measurements in many cases involve the use of satellites which can be referred to as geodetic satellites [12,13, 14, 15, 16, 17, 18, 19,20]. In this paper, the geodetic satellites considered are LAGEOS-1, JASON 3 and TANDEM X satellites [21, 22, 23, 24, 25, 26, 27, 28].

In any case, in order to be used for data capture on any given earth location, the satellite must be visible from that earth location. As such, satellite visibility determination is essential for its application on geodetic measurements [29,30, 31,32, 33,34]. The visibility time computation is used to determine the amount of time that the satellite is visible from earth [35, 36, 37, 38, 39, 40]. The visibility time is usually a fraction of the satellite's orbital period. Again, the visibility time determination depends on the nature or shape of the satellite orbit. For highly eccentric orbit, the eccentricity pays significant role in the determination of the visibility time [41,42,43,44,45]. However, for circular or near circular orbits with very low eccentricity values, the orbital altitude has much influence in the value of the visibility time [46,47].

Notably, the three satellites considered in this paper are of circular orbit with eccentricity in the range of 0.00451 to 0.00014 [48]. Accordingly, the analytical expressions for computing visibility time of circular orbits are applied. The analytical expression are derived with respect to the orbital altitude of the satellites. In addition, the visibility time of satellites are affected by restriction on the minimum zenith angle. Accordingly, in the analysis, the models used also accounted for the minimum zenith angle restriction. In all, the study in this paper presented the requisite parameters of the case study geodetic satellites and the analytical models for the visibility time along with numerical computations based on the case

study satellite parameters. Also, the visibility time of the case study satellites are compared for various zenith angle restrictions.

2. Methodology

2.1 Development of the analytical model for the visibility time computation

The visibility time is derived with respect to ρ, which is the ratio of the earth radius (R_e) to the satellite radius (R_s) where R_s is expressed in terms of orbital altitude or orbital height (h) and R_e as follows;

$$R_s = R_e + h \quad (1)$$

$$\rho = \frac{R_e}{R_e+h} \quad (2)$$

Consider the diagram for a circular orbit satellite visibility time with restriction on the minimal zenith angle, φ, as shown in Figure 1. The angle for one round trip on the circular orbit is 2π radians. Without restriction on the minimum zenith angle (φ), (in Figure 1) the visibility angle is $2(\beta_1)$ where;

$$\text{Cos}(\beta_1) = \frac{OP}{OW} = \frac{R_e}{R_e+h} = \rho \quad (3)$$

With restriction on the minimum zenith angle (φ), (in Figure 1) the visibility angle is $2(\beta_2)$, where;

$$\text{Cos}(\beta_2) = \frac{OG}{OY} = \frac{OG}{OW} \quad (4)$$

$$\text{Sin}(\beta_2) = \frac{GY}{OY} = \frac{GY}{OW} \quad (5)$$

$$\text{Tan}(\varphi) = \frac{GY}{PG} = \frac{GY}{PG} \quad (6)$$

$$\frac{1}{\text{Tan}(\varphi)} = \frac{PG}{GY} \quad (7)$$

$$\left(\frac{1}{\text{Tan}(\varphi)}\right)\text{Sin}(\beta_2) = \left(\frac{PG}{GY}\right)\left(\frac{GY}{OW}\right) = \frac{PG}{OW} \quad (8)$$

$$\left(\frac{1}{\text{Tan}(\varphi)}\right)\text{Sin}(\beta_2) = \frac{PG}{OW} \quad (9)$$

$$\text{Cos}(\beta_2) - \left(\frac{1}{\text{Tan}(\varphi)}\right)\text{Sin}(\beta_2) = \frac{OG}{OW} - \frac{PG}{OW} \quad (10)$$

$$\text{Cos}(\beta_2) - \left(\frac{1}{\text{Tan}(\varphi)}\right)\text{Sin}(\beta_2) = \frac{OG-PG}{OW} \quad (11)$$

But from Figure 1,

$$OG - PG = OP = R_e \quad (12)$$

$$OW = R_e + h \quad (13)$$

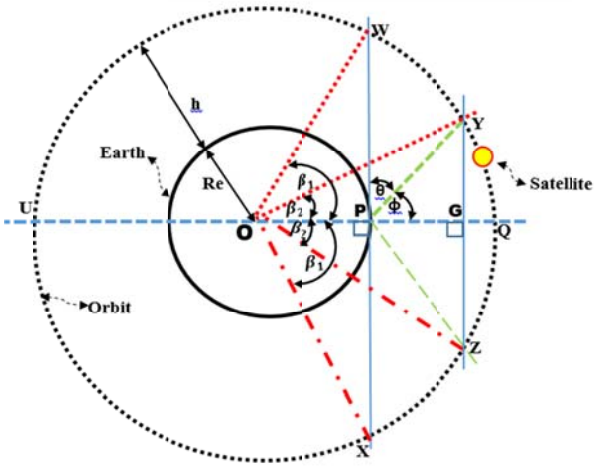

Figure 1 The diagram for a circular orbit satellite visibility time with restriction on the minimal zenith angle, φ

Hence;

$$\text{Cos}(\beta_2) - \left(\frac{1}{\text{Tan}(\varphi)}\right)\text{Sin}(\beta_2) = \frac{OP}{OW} = \frac{R_e}{R_e+h} = \rho \quad (14)$$

Now, let

$$\text{Z} = \frac{1}{\text{Tan}(\varphi)} \quad (15)$$

Where

$$\varphi = 90 - \varphi \text{ if } \varphi \text{ and } \varphi \text{ are in degree} \quad (16)$$

$$\varphi = (\pi/2) - \varphi \text{ if } \varphi \text{ and } \varphi \text{ are in radians} \quad (17)$$

Then,

$$\beta_2 = 2\left(\text{Tan}^{-1}\left(\frac{\sqrt{(1+Z^2-\rho^2)}-Z}{1+\rho}\right)\right) \quad (18)$$

Also, the time one round trip on the circular orbit is the satellite orbital period, T_o, where

$$T_o = 2\pi\sqrt{\frac{(R_e+h)^3}{\mu}} \text{ Seconds} \quad (19)$$

The visibility arc angle for the case with restriction on the minimum zenith angle is $2(\beta_2)$radians

The visibility time angle is denoted as Δt_v , then;

$$\frac{\Delta t_v}{T_o} = \frac{2(\beta_2)}{2\pi} \quad (20)$$

$$\Delta t_v = \left(\frac{2(\beta_2)}{2\pi}\right)T_o = \left(\frac{\beta_2}{\pi}\right)T_o = (2\beta_2)\sqrt{\frac{(R_e+h)^3}{\mu}} \text{ Seconds} \quad (21)$$

$$\Delta t_v = \left(4\left(\text{Tan}^{-1}\left(\frac{\sqrt{(1+Z^2-\rho^2)}-Z}{1+\rho}\right)\right)\right)\sqrt{\frac{(R_e+h)^3}{\mu}} \text{ Seconds} \quad (22)$$

The satellite visibility time can be expressed in minutes (denoted as Δt_{vM}) and in hours(denoted as Δt_{vH}) where ;

$$\Delta t_{\text{vMin}} = \frac{\Delta t_v}{60} \quad (23)$$

$$\Delta t_{\text{vHour}} = \frac{\Delta t_v}{3600} \quad (24)$$

2.2 The case study satellites

The numerical examples in this paper are presented with respect to three geodetic satellites, namely; LAGEOS-1 , JASON 3 and TANDEM X [48]. The launch details and some orbital elements of the three satellites are presented in Table 1. The analytical model for the visibility time computation in this paper shows that variations in the visibility time from one satellite to another is mainly dependent on the orbital altitude or orbital height (h) of the satellite. Also, it is known from orbital track prediction data of satellites varies with time. However, the satellite mean altitude over an orbital period or over a given timeframe is used to compute the visibility time. The variations in the mean altitude of the selected satellites are shown in Figure 1, Figure 2 , Figure 3 and Figure 4. The data on orbital period and orbital altitude of the case study satellites are presented in Table 2. The data in Table 2 shows that the orbital altitude of the Lageos-1 satellite is about 11.6 times that of the TanDEM-X satellite while that of Jason-3 satellite is about 2.6 times the altitude of the TanDEM-X satellite.

Table 1 The launch details and some orbital elements of the three geodetic satellites, namely; LAGEOS-1 , JASON 3 and TANDEM X Source: [48]

Launch Details	LAGEOS-1	JASON 3	TANDEM X
Owner	United States	United States	Germany
NORAD ID	8820	41240	36605
COSPAR ID	1976-039A	2016-002A	2010-030A
Orbital elements	LAGEOS-1	JASON 3	TANDEM X
Inclination	109.861°	66.044°	97.445°
Eccentricity	0.00451	0.00081	0.00014
RA ascending node	1.551 hr	1.506 hr	8.728 hr
Argument perihelion	264.596°	273.463°	110.102°
Mean anomaly	153.179°	86.546°	27.029°
Orbital period	225.470 mi n	112.418 mi n	94.790 mi n
Epoch of osculation	02 May 2022, 12:52	03 May 2022, 10:14	02 May 2022, 16:15
Source:	[48]		

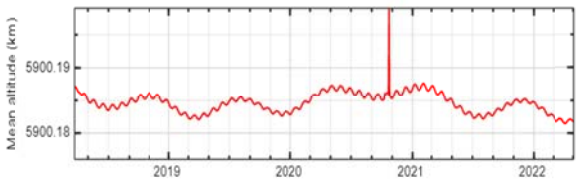

I. FIGURE 1 MEAN ALTITUDE OF LAGEOS-1 SATELLITE

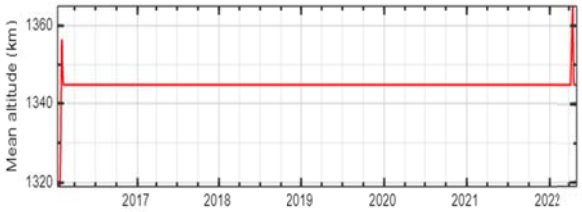

Figure 2 Mean altitude of JASON 3 satellite

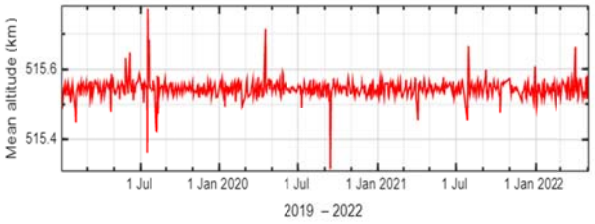

Figure 3 Mean altitude of TANDEM X satellite

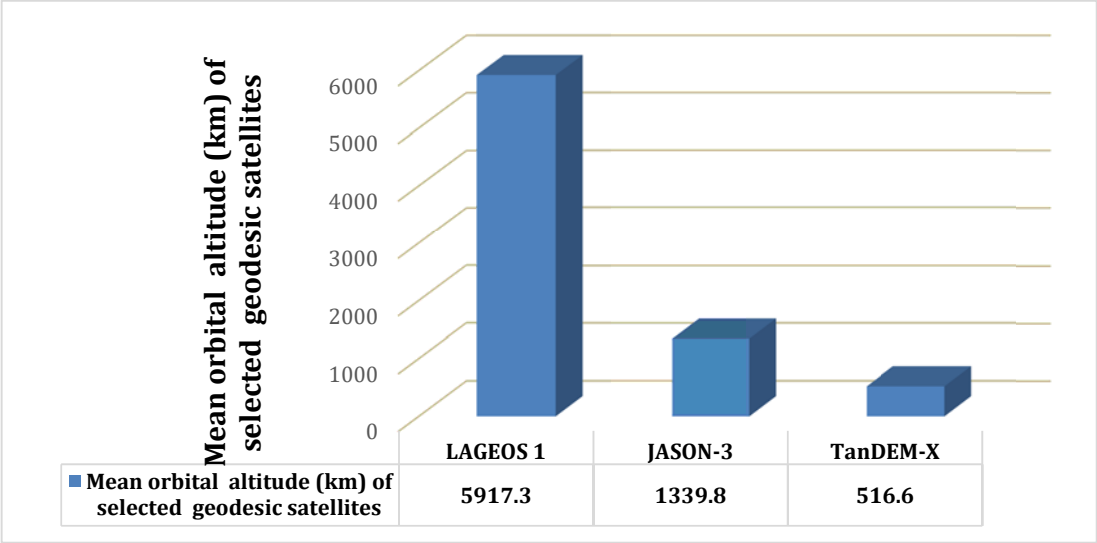

Figure 4 The mean altitude of the three case study satellites

Table 2 The data on orbital period and orbital altitude of the case study satellites

Geodesic Satellites	Orbital Period, To (Min)	Orbital altitude, h (km) from the orbital period data in Table 1	Orbital altitude, h (km) from the mean orbital altitude data in Figure 4	Normalised orbital altitude with respect to that of TanDEM-X satellite
LAGEOS-1	225.470	5,893.03	5917.3	11.5
JASON-3	112.418	1,337.71	1339.8	2.6
TanDEM-X	94.790	508.41	516.6	1

3. Results and Discussion

The visibility time analysis is conducted using the data on orbital altitude of the case study satellites as presented in Table 2. The results of the visibility time computations for the LAGEOS-1 satellite are shown in Table 3, the results for JASON-3 satellites are shown in Table 4 and the results for TanDEM-X satellites are shown in Table 5.

The results show that with minimum zenith angle restriction value of 0°, the Lageos-1 satellite has the maximum visibility time of 73.5 minutes along with the highest visibility angle of 58.7°. The visibility time and visibility angle of the Lageos-1 satellite drop to 51.1 minutes and 40.8° at minimum zenith angle restriction value of 20°. The analytical model that relates the visibility time of Lageos-1 satellite with the minimum zenith angle restriction in degree is given as;

$$\text{Lageos-1 } \Delta tv = 0.0068\varphi^2 - 1.2552\varphi + 73.497 \quad (25)$$

Similar models for the Jason-3 and TanDEM-X satellites are given as;

$$\text{Jason-3 } \Delta tv = 0.0073\varphi^2 - 0.6196\varphi + 21.386 \quad (26)$$

$$\text{TanDEM-X} = 0.0086\varphi^2 - 0.5033\varphi + 11.657 \quad (27)$$

Among the three geodesic satellites considered, TanDEM-X satellite with the lowest altitude has the lowest visibility time. However, while the ratio of the orbital altitude of the Lageos-1 satellite to the altitude of the TanDEM-X satellite is about 11.6 and that of Jason-3 altitude to TanDEM-X altitude is about 2.6, the ratio of the visibility time varies with the minimum zenith angle restriction, as shown in Table 6 and Figure 8. For the Lageos-1 satellite, the ratio of the visibility time to that of the TanDEM-X satellite ranges from 6.3 at minimum zenith angle of 0º to 10.2 at minimum zenith angle of 20°. Also, for the Jason-3 satellite, the ratio of the visibility time to that of the TanDEM-X satellite ranges from 1.8 at minimum zenith angle of 0º to 2.4 at minimum zenith angle of 20°.

In all, the results show that the higher the orbital altitude, the higher the visibility time of the satellite. Also, the minimum zenith angle restriction significantly affect the visibility time of the satellite; notably, the visibility time decreases as the value of minimum zenith angle restriction increases.

Table 3 The results of the visibility time computations for the LAGEOS-1 satellite

Satellite	Orbital altitude, h (km)	Minimal Zenith Angle Restriction , φ(degree)	Orbital Period , To (Min)	Visibility Time, Δtv (min)	Ratio of To/Δtv	Visibility Angle , Δtv (degree)	Percentage change in visibility angle (%)
LAGEOS-1	5893.03	0.0	225.5	73.5	0.326	58.7	0.0
LAGEOS-1	5893.03	2.0	225.5	71.0	0.315	56.7	-3.4
LAGEOS-1	5893.03	4.0	225.5	68.6	0.304	54.8	-6.7
LAGEOS-1	5893.03	6.0	225.5	66.2	0.294	52.9	-9.9
LAGEOS-1	5893.03	8.0	225.5	63.9	0.283	51.0	-13.1
LAGEOS-1	5893.03	10.0	225.5	61.6	0.273	49.2	-16.1
LAGEOS-1	5893.03	12.0	225.5	59.4	0.264	47.4	-19.2
LAGEOS-1	5893.03	14.0	225.5	57.3	0.254	45.7	-22.1
LAGEOS-1	5893.03	16.0	225.5	55.1	0.245	44.0	-25.0
LAGEOS-1	5893.03	18.0	225.5	53.1	0.235	42.4	-27.8
LAGEOS-1	5893.03	20.0	225.5	51.1	0.226	40.8	-30.5

Table 4 The results of the visibility time computations for the JASON-3 satellite

Satellite	Orbital altitude, h (km)	Minimal Zenith Angle Restriction , φ(degree)	Orbital Period , To (Min)	Visibility Time, Δtv (min)	Ratio of To/Δtv	Visibility Angle , Δtv (degree)	Percentage change in visibility angle (%)
JASON-3	1337.71	0.0	112.4	21.4	0.190	34.2	0.0
JASON-3	1337.71	2.0	112.4	20.2	0.179	32.3	-5.7
JASON-3	1337.71	4.0	112.4	19.0	0.169	30.5	-11.1
JASON-3	1337.71	6.0	112.4	17.9	0.159	28.7	-16.2
JASON-3	1337.71	8.0	112.4	16.9	0.150	27.1	-21.0
JASON-3	1337.71	10.0	112.4	15.9	0.142	25.5	-25.5
JASON-3	1337.71	12.0	112.4	15.0	0.134	24.0	-29.8
JASON-3	1337.71	14.0	112.4	14.2	0.126	22.7	-33.8
JASON-3	1337.71	16.0	112.4	13.4	0.119	21.4	-37.6

JASON-3	1337.71	18.0	112.4	12.6	0.112	20.2	-41.1
JASON-3	1337.71	20.0	112.4	11.9	0.106	19.0	-44.4

Table 5 The results of the visibility time computations for the TanDEM-X satellite

Satellite	Orbital altitude, h (km)	Minimal Zenith Angle Restriction , φ(degree)	Orbital Period , To (Min)	Visibility Time, Δtv (min)	Ratio of Δtv / To	Visibility Angle , Δtv (degree)	Percentage change in visibility angle (%)
TanDEM-X	508.41	0.0	94.8	11.7	0.123	22.2	0.0
TanDEM-X	508.41	2.0	94.8	10.7	0.112	20.2	-8.6
TanDEM-X	508.41	4.0	94.8	9.7	0.103	18.5	-16.5
TanDEM-X	508.41	6.0	94.8	8.9	0.094	16.9	-23.7
TanDEM-X	508.41	8.0	94.8	8.2	0.086	15.5	-30.1
TanDEM-X	508.41	10.0	94.8	7.5	0.079	14.2	-35.9
TanDEM-X	508.41	12.0	94.8	6.9	0.073	13.1	-41.1
TanDEM-X	508.41	14.0	94.8	6.3	0.067	12.0	-45.8
TanDEM-X	508.41	16.0	94.8	5.8	0.062	11.1	-49.9
TanDEM-X	508.41	18.0	94.8	5.4	0.057	10.3	-53.7
TanDEM-X	508.41	20.0	94.8	5.0	0.053	9.5	-57.1

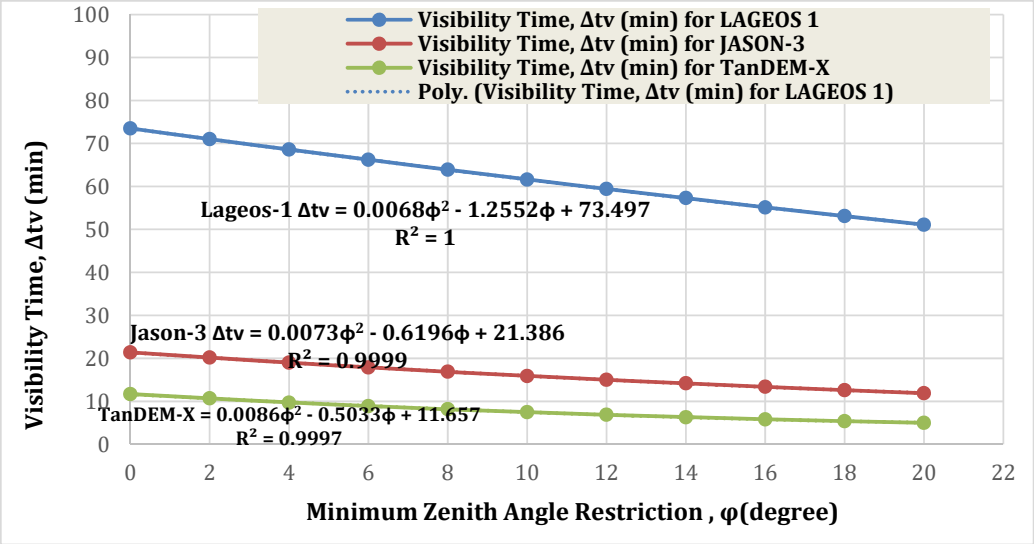

Figure 5 The graph of visibility time versus minimum zenith angle restriction for the three geodesic satellites

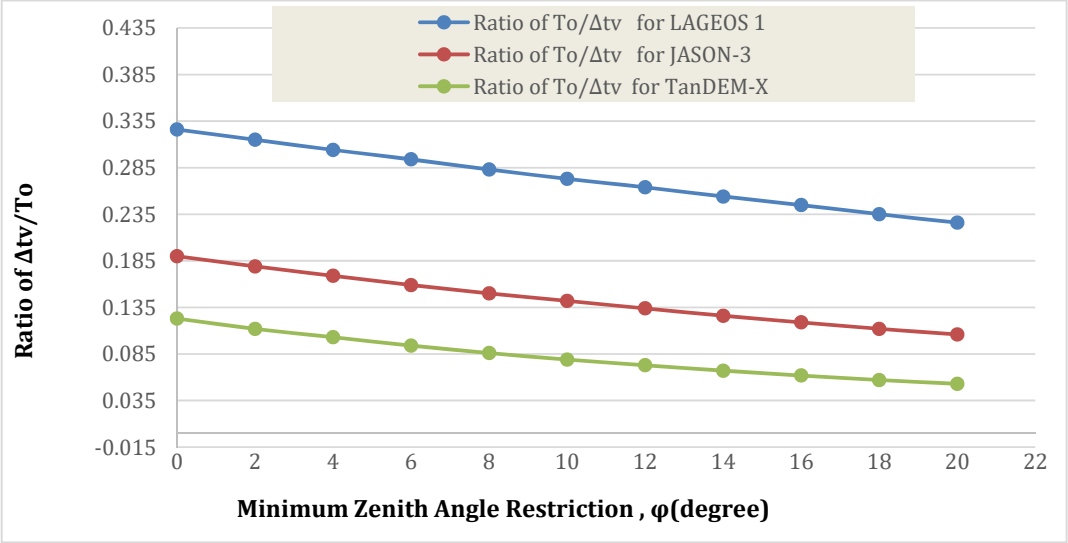

Figure 6 The graph of ration of visibility time to orbital period versus minimum zenith angle restriction for the three geodesic satellites

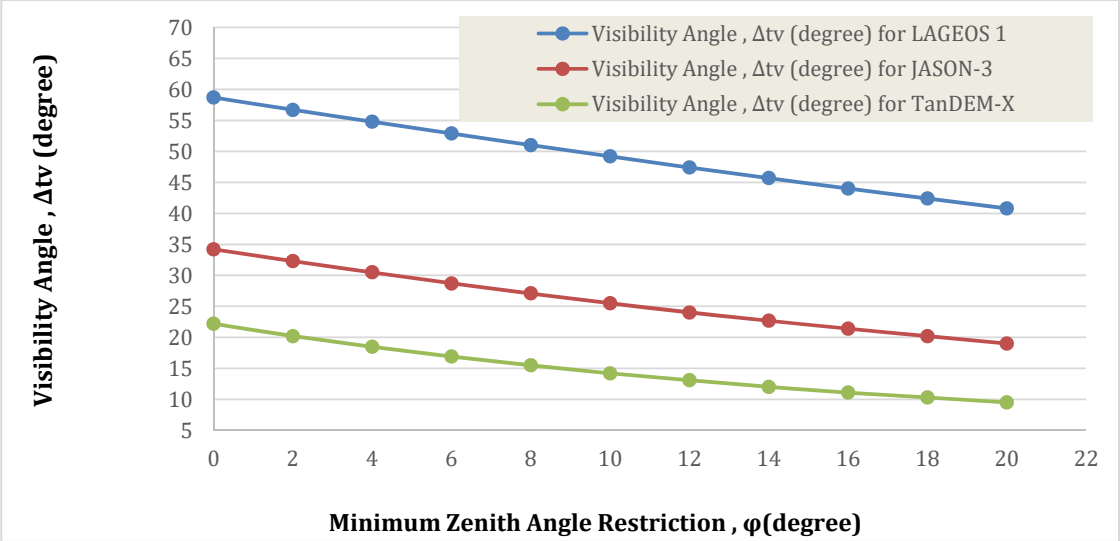

Figure 7 The graph of visibility angle versus minimum zenith angle restriction for the three geodesic satellites

Table 6 The ratio of the visibility time and ratio of orbital altitude with respect to that of the TanDEM-X satellite

Ratio of the visibility time of Lageos-1 satellite to the visibility time of the TanDEM-X satellite	Ratio of the visibility time of Jason-3 satellite to the visibility time of the TanDEM-X satellite	Ratio of the orbital altitude of Lageos-1 satellite to the altitude of the TanDEM-X satellite	Ratio of the orbital altitude of Jason-3 satellite to the altitude of the TanDEM-X satellite
6.3	1.8	11.6	2.6
6.6	1.9	11.6	2.6
7.1	2.0	11.6	2.6
7.4	2.0	11.6	2.6
7.8	2.1	11.6	2.6
8.2	2.1	11.6	2.6
8.6	2.2	11.6	2.6
9.1	2.3	11.6	2.6
9.5	2.3	11.6	2.6
9.8	2.3	11.6	2.6
10.2	2.4	11.6	2.6

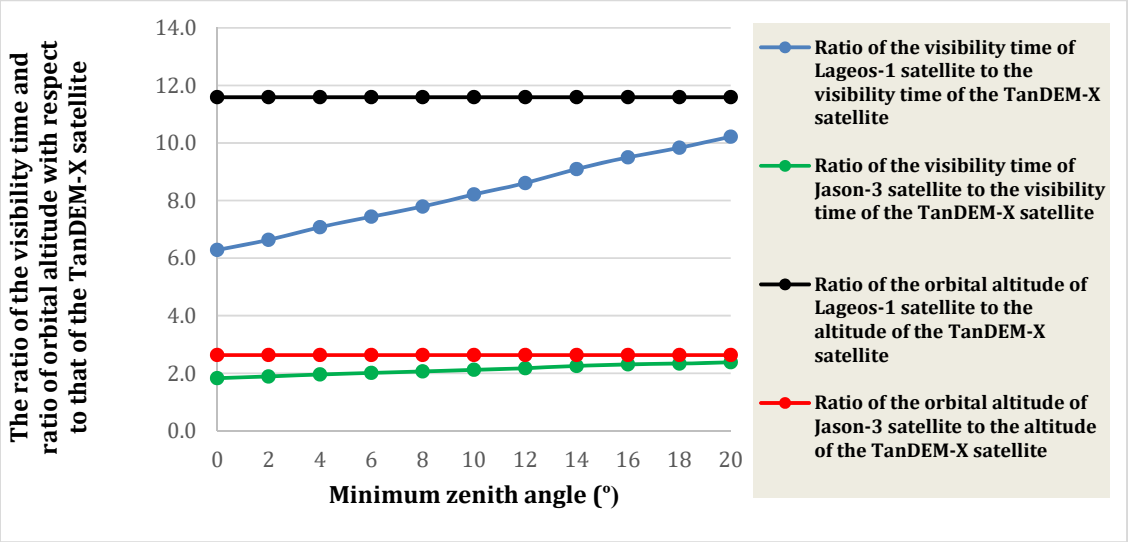

Figure 8 The graph of ratio of the visibility time and ratio of orbital altitude as function of minimum zenith angle restriction

4. Conclusion

The visibility time of geodesic satellites is studied. The study presented the analytical expressions that are used in the computation of the orbital period as well as the visibility angle and the visibility time subject to certain minimum zenith angle. Three case study geodesic satellites were used in the numerical examples and the results showed that the higher the orbital altitude, the higher the visibility time of the satellite. Also, the minimum zenith angle restriction significantly affect the visibility time of the satellite; notably, the visibility time decreases as the value of minimum zenith angle restriction increases.

References

1. Vanicek, P., & Krakiwsky, E. J. (2015). *Geodesy: the concepts*. Elsevier.
2. Ince, E. S., Barthelmes, F., Reißland, S., Elger, K., Förste, C., Flechtner, F., & Schuh, H. (2019). ICGEM–15 years of successful collection and distribution of global gravitational models, associated services, and future plans. *Earth System Science Data*, *11*(2), 647-674.
3. Torge, W., & Müller, J. (2012). Geodesy. In *Geodesy*. de Gruyter.
4. Herring, T. A. (1999). Geodetic applications of GPS. *Proceedings of the IEEE*, *87*(1), 92-110.
5. Blewitt, G., Altamimi, Z., Davis, J., Gross, R., Kuo, C. Y., Lemoine, F. G., ... & Zerbini, S. (2010). Geodetic observations and global reference frame contributions to understanding sea-level rise and variability. *Understanding sea-level rise and variability*, 256-284.
6. Freeden, W., & Schreiner, M. (2020). Mathematical Geodesy. In *Mathematische Geodäsie/Mathematical Geodesy* (pp. 3-63). Springer Spektrum, Berlin, Heidelberg.
7. Freymueller, J. T. (2021). GPS, tectonic geodesy. In *Encyclopedia of Solid Earth Geophysics* (pp. 558-578). Cham: Springer International Publishing.
8. Sjöberg, L. E., & Bagherbandi, M. (2017). *Gravity inversion and integration*. Basel, Switzerland: Springer International Publishing AG.
9. Bock, Y., & Melgar, D. (2016). Physical applications of GPS geodesy: A review. *Reports on Progress in Physics*, *79*(10), 106801.
10. Yibin, Y. A. O., Yuanxi, Y. A. N. G., Heping, S. U. N., & Jiancheng, L. I. (2020). Geodesy discipline: progress and perspective. *Acta Geodaetica et Cartographica Sinica*, *49*(10), 1243.
11. Jin, S. (Ed.). (2014). *Planetary geodesy and remote sensing*. CRC Press.
12. Pearlman, M., Arnold, D., Davis, M., Barlier, F., Biancale, R., Vasiliev, V., ... & Bloßfeld, M. (2019). Laser geodetic satellites: a high-accuracy scientific tool. *Journal of Geodesy*, *93*(11), 2181-2194.
13. Otsubo, T., & Appleby, G. M. (2003). System-dependent center-of-mass correction for spherical geodetic satellites. *Journal of Geophysical Research: Solid Earth*, *108*(B4).
14. Seeber, G. (2008). Satellite geodesy. In *Satellite Geodesy*. de Gruyter.
15. Kaula, W. M. (2013). *Theory of satellite geodesy: applications of satellites to geodesy*. Courier Corporation.
16. Tourian, M. J., Elmi, O., Shafaghi, Y., Behnia, S., Saemian, P., Schlesinger, R., & Sneeuw, N. (2022). HydroSat: geometric quantities of the global water cycle from geodetic satellites. *Earth System Science Data*, *14*(5), 2463-2486.
17. Giorgi, G., Schmidt, T. D., Trainotti, C., Mata-Calvo, R., Fuchs, C., Hoque, M. M., ... & Schuh, H. (2019). Advanced technologies for satellite navigation and geodesy. *Advances in Space Research*, *64*(6), 1256-1273.

18. Sośnica, K. (2014). *Determination of precise satellite orbits and geodetic parameters using satellite laser ranging*. Astronomical Institute, University of Bern, Switzerland.
19. Bloßfeld, M., Rudenko, S., Kehm, A., Panafidina, N., Müller, H., Angermann, D., ... & Seitz, M. (2018). Consistent estimation of geodetic parameters from SLR satellite constellation measurements. *Journal of Geodesy*, *92*(9), 1003-1021.
20. Appleby, G., Rodríguez, J., & Altamimi, Z. (2016). Assessment of the accuracy of global geodetic satellite laser ranging observations and estimated impact on ITRF scale: estimation of systematic errors in LAGEOS observations 1993–2014. *Journal of Geodesy*, *90*(12), 1371-1388.
21. Strugarek, D., Sośnica, K., Arnold, D., Jäggi, A., Zajdel, R., Bury, G., & Drożdżewski, M. (2019). Determination of global geodetic parameters using Satellite Laser Ranging measurements to Sentinel-3 satellites. *Remote sensing*, *11*(19), 2282.
22. Strugarek, D., Sośnica, K., Arnold, D., Jäggi, A., Zajdel, R., & Bury, G. (2021). Determination of SLR station coordinates based on LEO, LARES, LAGEOS, and Galileo satellites. *Earth, Planets and Space*, *73*(1), 1-21.
23. Arnold, D., Montenbruck, O., Hackel, S., & Sośnica, K. (2019). Satellite laser ranging to low Earth orbiters: orbit and network validation. *Journal of geodesy*, *93*(11), 2315-2334.
24. Montenbruck, O., Kahle, R., D'Amico, S., & Ardaens, J. S. (2008). Navigation and control of the TanDEM-X formation. *The Journal of the Astronautical Sciences*, *56*(3), 341-357.
25. Biancamaria, S., Schaedele, T., Blumstein, D., Frappart, F., Boy, F., Desjonquères, J. D., ... & Niño, F. (2018). Validation of Jason-3 tracking modes over French rivers. *Remote Sensing of Environment*, *209*, 77-89.
26. Grunwaldt, L. (2008, June). The TOR Payload on TanDEM-X. In *7th European Conference on Synthetic Aperture Radar* (pp. 1-3). VDE.
27. Wang, J., Xu, H., Yang, L., Song, Q., & Ma, C. (2021). Cross-Calibrations of the HY-2B Altimeter Using Jason-3 Satellite During the Period of April 2019–September 2020. *Frontiers in Earth Science*, *9*, 215.
28. Jia, Y., Yang, J., Lin, M., Zhang, Y., Ma, C., & Fan, C. (2020). Global assessments of the HY-2B measurements and cross-calibrations with Jason-3. *Remote Sensing*, *12*(15), 2470.
29. Dawidowicz, K., & Krzan, G. (2014). Accuracy of single receiver static GNSS measurements under conditions of limited satellite availability. *Survey review*, *46*(337), 278-287.
30. Hackel, S., Montenbruck, O., Steigenberger, P., Balss, U., Gisinger, C., & Eineder, M. (2017). Model improvements and validation of TerraSAR-X precise orbit determination. *Journal of Geodesy*, *91*(5), 547-562.
31. Gao, Y., Gao, Y., Liu, B., & Jiang, Y. (2021). Enhanced fault detection and exclusion based on Kalman filter with colored measurement noise and application to RTK. *GPS Solutions*, *25*(3), 1-13.
32. Alkan, R. M., Saka, M. H., Ozulu, İ. M., & İlçi, V. (2017). Kinematic precise point positioning using GPS and GLONASS measurements in marine environments. *Measurement*, *109*, 36-43.
33. Lee, B., Lee, Y. J., & Sung, S. (2018). An efficient integrated attitude determination method using partially available doppler measurement under weak GPS environment. *International Journal of Control, Automation and Systems*, *16*(6), 3000-3012.
34. Steigenberger, P., Thoelert, S., & Montenbruck, O. (2018). GNSS satellite transmit power and its impact on orbit determination. *Journal of Geodesy*, *92*(6), 609-624.
35. Katona, Z., & Donner, A. (2008, October). On mean visibility time of non-repeating satellite orbits. In *2008 IEEE International Workshop on Satellite and Space Communications* (pp. 247-251). IEEE.
36. Katona, Z. (2010, September). On mean revisit frequency of non-repeating satellite orbits with finite sensor range. In *2010 5th Advanced Satellite Multimedia Systems Conference and the 11th Signal Processing for Space Communications Workshop* (pp. 369-374). IEEE.
37. Han, C., Gao, X., & Sun, X. (2017). Rapid satellite-to-site visibility determination based on self-adaptive interpolation technique. *Science China Technological Sciences*, *60*(2), 264-270.
38. Graven, A. J., & Lo, M. W. (2020). The Long-Term Forecast of Station View Periods for Elliptical Orbits. *arXiv preprint arXiv:2010.06021*.
39. Katona, Z. (2010, June). On mean visibility time of non-repeating satellite orbits with finite sensor range. In *2010 Second International Conference on Advances in Satellite and Space Communications* (pp. 157-162). IEEE.
40. Ali, I., Al-Dhahir, N., & Hershey, J. E. (1999). Predicting the visibility of LEO satellites. *IEEE Transactions on Aerospace and Electronic Systems*, *35*(4), 1183-1190.

41. Asmus, V. V., Dyadyuchenko, V. N., Nosenko, Y. I., Polishchuk, G. M., & Selin, V. A. (2007). A highly elliptical orbit space system for hydrometeorological monitoring of the Arctic region. *Bulletin of the World Meteorological Organization*, *56*(4), 293-296.
42. Ciceri, S., Lillo-Box, J., Southworth, J., Mancini, L., Henning, T., & Barrado, D. (2015). Kepler-432 b: a massive planet in a highly eccentric orbit transiting a red giant. *Astronomy & Astrophysics*, *573*, L5.
43. Thao, P. C., Mann, A. W., Johnson, M. C., Newton, E. R., Guo, X., Kain, I. J., ... & Kraus, A. L. (2020). Zodiacal exoplanets in time (ZEIT). IX. A flat transmission spectrum and a highly eccentric orbit for the young Neptune K2-25b as revealed by Spitzer. *The Astronomical Journal*, *159*(1), 32.
44. Silha, J., Schildknecht, T., Hinze, A., Flohrer, T., & Vananti, A. (2017). An optical survey for space debris on highly eccentric and inclined MEO orbits. *Advances in space research*, *59*(1), 181-192.
45. Ciceri, S., Lillo-Box, J., Southworth, J., Mancini, L., Henning, T., & Barrado, D. (2014). KOI-1299b: a massive planet in a highly eccentric orbit transiting a red giant. *arXiv preprint arXiv:1410.2999*.
46. Capderou, M. (2002). *Satellites: orbites et missions. Chapter 5 Orbit and Ground Track of a Satellite*. Springer Science & Business Media.
47. Satellite Visibility Prediction (2002). In: Doppler Applications in LEO Satellite Communication Systems. The International Series in Engineering and Computer Science, vol 656. Springer, Boston, MA. https://doi.org/10.1007/0-306-47546-4_4
48. **https://in-the-sky.org**